Research on Resonant Wireless Energy Supply Double-Layer Receiving Coupler for Portable Electronic Equipment

Weihua Chen*, Kun Qian*, and Xiaoheng Yan

Abstract—In order to reduce the electromagnetic interference on the receiving side of electronic equipment in the process of wireless energy supply, a magnetic coupling resonant wireless energy supply system for portable electronic equipment with double-layer PCB coil structure is designed under 100 kHz. Firstly, the circuit principle is analyzed, and the LCC-P compensation circuit model is established. Then, the coil model is constructed. The effects of turns and wire diameter on the coil self inductance and coupling coefficient are analyzed. The best parameters are selected, and the magnetic field distributions of the three coil structures at different distances are simulated and studied. Finally, an experimental platform is built to study the transmission efficiencies of different receiving coils with different spacings. The magnetic field intensitiwa at different positions are compared to further verify the performance of double-layer coils. The experimental results show that when the coil spacing is in the range of 4–16 mm, the efficiency of the WPT system can reach 40%–71%. The strength of the central magnetic field of the coil is increased by 16%, and the external magnetic field is reduced by more than 20%. The temperature rise of one hour charging is 5.34°, which is only 0.78° higher than that of other coils.

1. INTRODUCTION

In recent years, due to its convenience and safety advantages, wireless power transfer (WPT) technology has been widely used in various fields such as electric vehicles (EVs) [1, 2], portable devices [3, 4], and implant technologies [5, 6]. In various studies conducted on wireless power supply for portable electronic devices, issues such as transmission efficiency and electromagnetic safety must be focused on. Therefore, many scholars have conducted extensive research on aspects such as improving energy supply efficiency and optimizing the safety and design of the coil structure [7–16].

To attenuate the electromagnetic interference on the receiving side of the WPT system during energy supply, many scholars have carried out research on such issues by using materials to shield the magnetic field. However, problems such as severe coil heating, high costs, too large size, and overweight still exist [17–19]. The design of the coil plays an important role in obtaining good system performance.

With improvements in printed circuit board (PCB) manufacturing technology, printed spiral coils (PSCs) can guarantee precise parameters and offer a wide range of connection options [20–22]. In 2018, Seungtaek's team designed a wireless charging system in a smartwatch strap with a PCB coil, shielding material, and a receiving circuit and proposed a flexible PCB coil model with 40 mm bending radius. However, the overall transmission efficiency of the system was low [23]. In 2020, Yi et al. proposed a new efficient antisymmetric planar coil to improve the performance of self-resonant coils. They are often used in high-frequency and low-power applications [24]. The improvement of PCB manufacturing process allows for a wide range of connections and configurations for the design of printed spiral coils. The PCB coils also have good consistency of parameters, which makes the coils ideal for a wide range

of applications. Therefore, the study of wireless energy transmission systems based on spiral printed coils at low frequencies is a good guide for engineering designs.

In summary, this paper designs a magnetically coupled resonant wireless energy supply system with a double-layer PCB coil structure at 100 kHz for portable electronic devices. The coil model is established, and the influence of the turn number and wire diameter on the self-inductance and coupling coefficient of the coil are analyzed to lower the system cost and optimize the coupling mechanism, and the transmission efficiency is ensured.

2. DOUBLE LAYER RECEIVER COIL BASED LCC-P COMPENSATION CIRCUIT

Coupling mechanism usually refers to the transmitting coil at the energy transmitting end and the induction coil at the energy receiving end. The transmitting coil is responsible for generating a high intensity alternating magnetic field, while the induction coil acquires energy through magnetic field induction, and the coupling performance has a serious impact on the overall efficiency and power of the system.

In the wireless energy supply system for portable electronic devices, coupling mechanism is a key component of the system. There is no fixed standard size, and it needs to be designed according to the actual needs. Therefore, whether the design and optimization of the coupling mechanism are appropriate or not directly affects the transmission efficiency of the system [25].

Due to the size limitation of the secondary side, a double-layer PCB with spiral coil winding layout is designed to enhance the magnetic field strength between the coils. As shown in Fig. 1, a serial printed spiral coil structure is proposed for resonant wireless energy transmission systems, where the coils in series can enhance their own inductance and mutual inductance strength to meet the system's requirements for transmission power and transmission distance. The special winding of the additional coils can attenuate the external magnetic field. The receiving coils are located on the top and bottom layers of the PCB board. Figure 1 shows a cross-section of the magnetic field at the receiving end. The additional coils generate an induced voltage under the effect of the magnetic field of the transmission coils and produce a counteracting magnetic field in the coils.
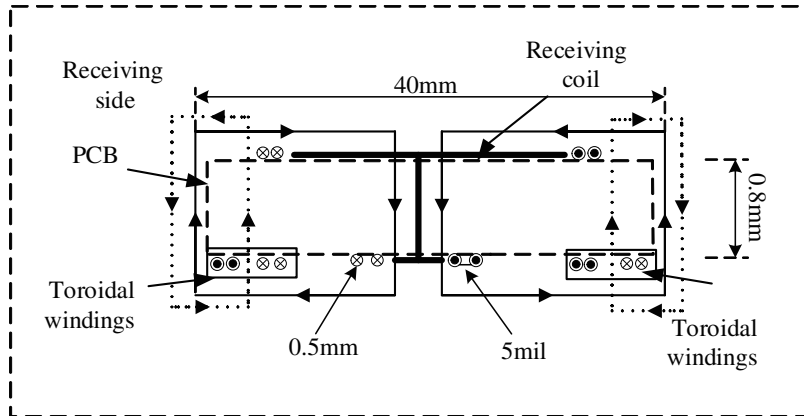

Figure 1. Side view of the magnetic flux distribution of the double layer PCB coil on the receiving side.

The established coil mutual inductance model is shown in Figure 2, where Tx and Rx denote the compensation networks corresponding to the transmitting and receiving coils, respectively, and Ax and Bx denote the compensation networks corresponding to the two additional coils. The transmitting coil consists of a series compensation inductor L_{11}, a parallel compensation capacitor C_1, and a series capacitor C_{11} on the primary side. The receiving coil consists of an equivalent resistor RL and a parallel compensated capacitor C_s. The additional coils are individually compensated by the corresponding C_a and C_b respectively to form a resonant circuit.
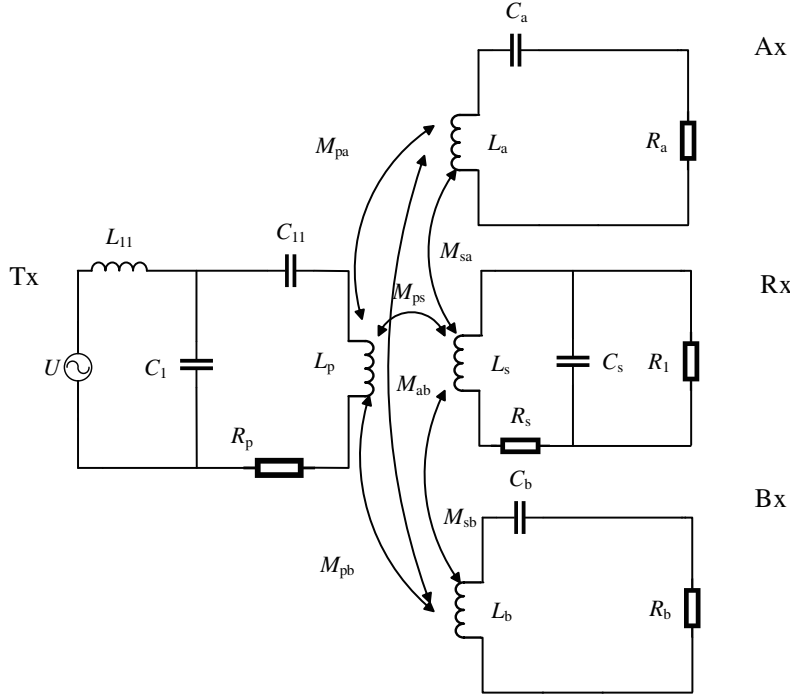
Figure 2. Model for mutual inductance of circuits with additional coils.

The subscripts p and s denote the primary and secondary circuits, respectively, and the subscripts a and b represent additional circuits. According to the Kirchhoff's voltage law (KVL), it can be concluded that:

$$\begin{bmatrix} U_p \\ 0 \\ 0 \\ 0 \end{bmatrix} = \begin{bmatrix} Z_p & j\omega M_{pa} & j\omega M_{pb} & j\omega M_{ps} \\ j\omega M_{pa} & Z_a & j\omega M_{ab} & j\omega M_{as} \\ j\omega M_{pb} & j\omega M_{ab} & Z_b & j\omega M_{bs} \\ j\omega M_{ps} & j\omega M_{as} & j\omega M_{bs} & Z_s \end{bmatrix} \tag{1}$$

Thus, the induced current can be obtained as:

$$\begin{cases} I_a = -\dfrac{j\omega^3(M_{bs}^2 M_{pa} - M_{ba}M_{bs}M_{ps} - M_{pb}M_{as}M_{bs}) + \omega^2(M_{as}M_{ps}Z_b + M_{ab}M_{pb}Z_s) + j\omega M_{pa}Z_bZ_s}{\omega^2(-2j\omega M_{as}M_{bs}M_{ab} + M_{as}^2 Z_b + M_{bs}^2 Z_a + M_{ab}^2 Z_s) + Z_aZ_bZ_s} I_p \\[2ex] I_b = -\dfrac{j\omega^3(M_{as}^2 M_{pb} - M_{ba}M_{as}M_{ps} - M_{pa}M_{as}M_{bs}) + \omega^2(M_{bs}M_{ps}Z_a + M_{ab}M_{pa}Z_s) + j\omega M_{pb}Z_aZ_s}{\omega^2(-2j\omega M_{as}M_{bs}M_{ab} + M_{as}^2 Z_b + M_{bs}^2 Z_a + M_{ab}^2 Z_s) + Z_aZ_bZ_s} I_p \\[2ex] I_s = -\dfrac{j\omega^3(M_{bs}^2 M_{ps} - M_{ba}M_{pa}M_{sb} - M_{ba}M_{pb}M_{sa}) + \omega^2(M_{pb}M_{sb}Z_a + M_{pa}M_{sa}Z_b) + j\omega M_{ps}Z_aZ_b}{\omega^2(-2j\omega M_{as}M_{bs}M_{ab} + M_{as}^2 Z_b + M_{bs}^2 Z_a + M_{ab}^2 Z_s) + Z_aZ_bZ_s} I_p \end{cases} \tag{2}$$

The system output power can be expressed as follows:

$$\begin{aligned} P_{out} &= \Re(I_s^2)R_1 \\ &= \left\{ \dfrac{j\omega^3(M_{bs}^2 M_{ps} - M_{ba}M_{pa}M_{sb} - M_{ba}M_{pb}M_{sa}) + \omega^2(M_{pb}M_{sb}R_a + M_{pa}M_{sa}R_b) + j\omega M_{ps}R_aR_b}{\omega^2[-2j\omega M_{as}M_{bs}M_{ab} + M_{as}^2 R_b + M_{bs}^2 R_a + M_{ab}^2(R_s + R_1)] + R_aR_b(R_s + R_1)} I_p \right\}^2 R_1 \end{aligned} \tag{3}$$

The efficiency of the system is:

$$\eta = \frac{P_{out}}{U_p I_p} \tag{4}$$

When the additional coil is decoupled from the receiving coil, the mutual inductance among the three coils is zero, and the currents induced by the receiving and additional coils by equation (2) have imaginary parts only. Both currents should therefore always lag 90° behind the transmitter current at the same time, regardless of the input signal. With the proposed winding direction, the direction of the current outside Ax is always opposite to the receiver pole plate, thus allowing an effective reduction of the magnetic field in the external area.

Thus, in this case, Equations (3)(4) can be further derived as:

$$P_{out} = \Re(I_s^2)R_1 = \left(\frac{j\omega M_{ps}}{R_s + R_1}I_p\right)^2 R_1 \tag{5}$$

$$\eta = \frac{P_{out}}{U_pI_p} = \left(\frac{j\omega M_{ps}}{R_1 + R_s}\right)^2 \frac{R_1}{Z_p} \tag{6}$$

Based on the above analysis, the resonant coil design is carried out on the printed circuit board from the design of the receiving coil and the additional coil compensated by the corresponding capacitor. The 100 kHz square wave generated by the full-bridge inverter circuit:

$$\omega = \frac{1}{\sqrt{L_{11}C_1}} = \frac{1}{\sqrt{L_sC_s}} = \sqrt{\frac{C_1 + C_{11}}{L_pC_1C_{11}}} = 2\pi f \tag{7}$$

3. COUPLING COIL MODEL AND PARAMETRIC ANALYSIS

3.1. Coil Modelling

Both receiving coils consist of two spiral coils on the top and bottom layers of a double-layer PCB, which are connected in series by a central joint. The PCB material between the top and bottom layers is FR4 with the thickness of 0.8 mm. The winding direction of the coils is shown in Figure 3. The additional coils are made up of two toroidal coils. The internal winding direction of the additional coil is the same as the winding direction of the receiving coil, while the external winding direction is opposite to the internal direction of the receiving coil.
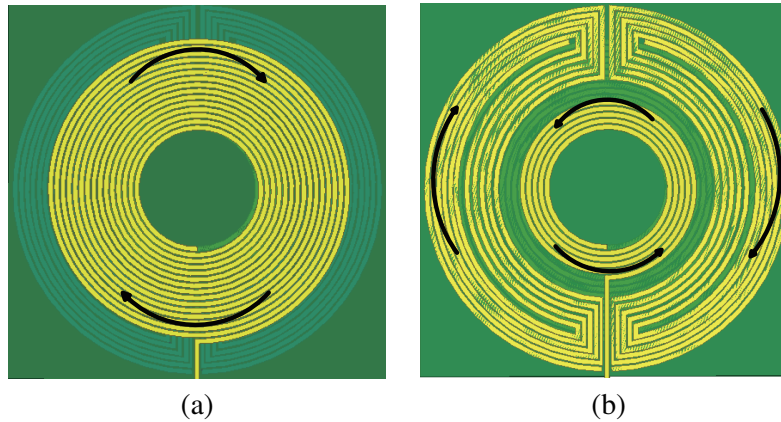

(a)   (b)

Figure 3. Proposed double layer PCB receiver coil with additional coils.

As a result, under the same excitation of the magnetic field, the induced current in the receiving coil is the same as the internal direction of the additional coil and opposite to the external direction, so that the flux densities in both external and internal areas of the receiving coil are attenuated. In other words, the useful flux is gathered in the central area of the coil, and the external flux is suppressed. The external flux tends to harm electronic components in other positions. Both windings of the additional coil are based on passive circuit elements, and no control or active components is involved. Another key point in the coil construction is the decoupling design. Due to the special winding orientation of

the proposed additional coils, it is possible to find the exact size and position relationship between the additional and receiving coils to decouple the coils, and design optimization is needed to acquire the goal. Decoupling is achieved when the positive value of the magnetic flux generated by the current of one coil is equal to the negative value of the magnetic flux generated by the other coil nearby itself. For the proposed double-layer receiver coil, the outer diameter of the additional coil must be slightly larger than the receiver coil in order to decouple the toroidal winding from the receiver coil in very close proximity. The parameters of different coils can be analyzed to achieve optimum flux density distribution, stable transmission efficiency, and minimal impact on the electronic devices with the decoupling characteristic.

3.2. Parametric Analysis

For the proposed double-layer receiver coil, characteristics of portable electronic devices such as thin, light, small space occupation, and high transmission efficiency need to be met. It is difficult to modify the parameters of the finished printed spiral coil, so it is particularly important to determine the inductance parameters of the coil in advance. Therefore, to address the characteristics and mutual constraints between the parameters in the coil design process, the influence of parameters such as the number of turns, wire spacing, wire width, and copper thickness of the coil should also be considered. These parameters have direct influence on the coil's performance indicators such as self-inductance L.

The coil optimization process is shown in Figure 4. The coupling mechanism used in portable electronic devices is mostly a single coil mechanism, and paper [26] shows that for single coil coupling mechanism, the coil shape is mainly circular or rectangular, while circular coil has a relatively high quality factor Q. As the effective winding length of the circular coil is smaller than that of the rectangular coil, the winding internal resistance is smaller than that of the rectangular coil. Considering the current carrying capacity of the coil, the two parameters are set based on the size of the inductance of the set coil and the specific application of the system. Based on existing PCB manufacturing technology, the
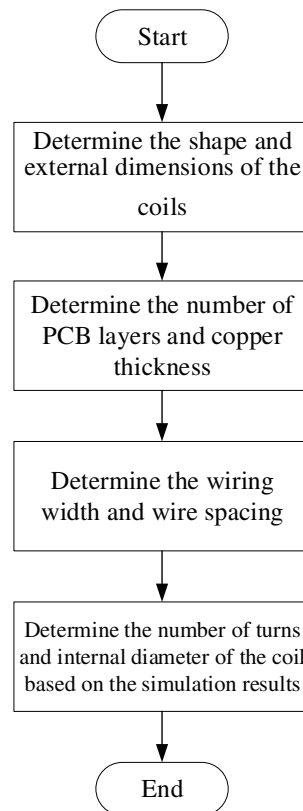

Figure 4. PCB coil parametric design analysis flowchart.

self-inductance and coupling coefficient of the coils are designed according to two variables: the number of turns N and the inner diameter of the coil, with the copper thickness of 1 oz and the wire spacing of 5 mil. The effects of the above parameters on the self and mutual inductances of the PCB coupling coil are calculated respectively for correlation analysis, providing basis for the design of the coupling mechanism.

If the outer diameter of the coil is determined, as shown in Figure 5, when the wire diameter is 0.5–0.8 mm, more coil turns can lead to the increase of self-inductance. For the same number of turns, the increase of the inner diameter caused by smaller wire diameter has relatively bigger effect on the self-inductance. As shown in Figure 6, the coupling coefficient gradually increases as the number of turns of the coil increases. The variation is less when the turn number is more than 15. The ANSYS Maxwell simulation shows that when the number of turns is 15, the coil meets the inductance requirements of the resonant coil and the space requirements of the PCB.
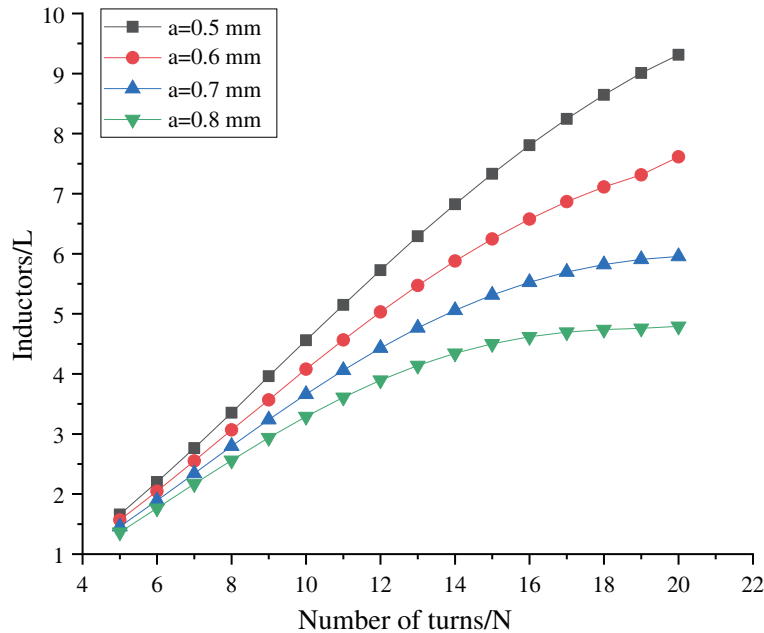

Figure 5. Effect of different number of turns and wire diameter on self-inductance.

4. SIMULATION

4.1. Simulation Setup

In order to verify the correctness of the above theoretical derivation, this paper uses the finite element simulation software ANSYS Maxwell to carry out simulation analysis. A model of the WPT transmission system is established on the simulation platform with an operating frequency of 100 kHz and an operating voltage of 5 V. The magnetic field around the receiving coil system is simulated, and the test points are set up as in Figure 7. The observation position is on the x-y plane with a distance of a horizontal coordinate of 40 mm from the center of the coil.

Simulations were carried out in the following cases: comparison of the magnetic field distributions of a single coil, a 15-turn, 5-turn series double layer coil, and a 15-turn, 5-turn series double layer coil with additional coils at distances of 4 mm, 7 mm, and 10 mm, and the variation of the magnetic field of the three coils in the plane was analyzed.
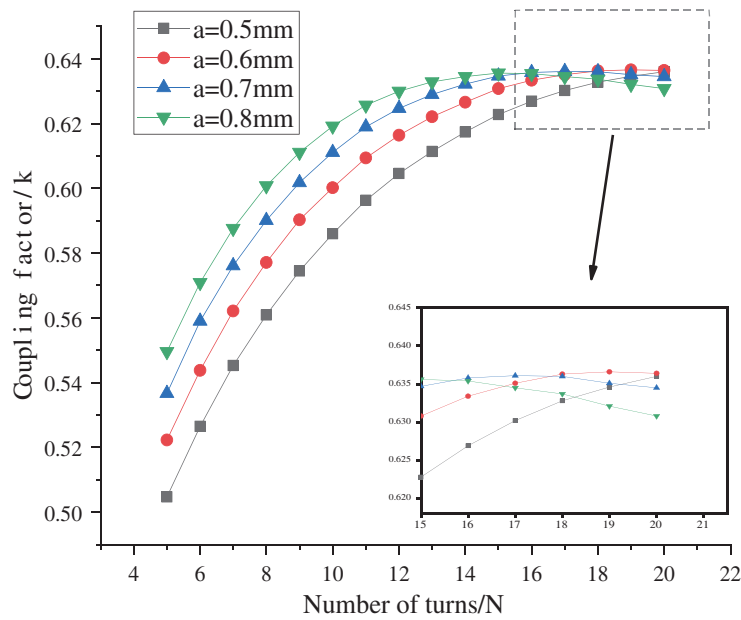
Figure 6. Effect of different number of turns and wire diameter on coupling coefficient.
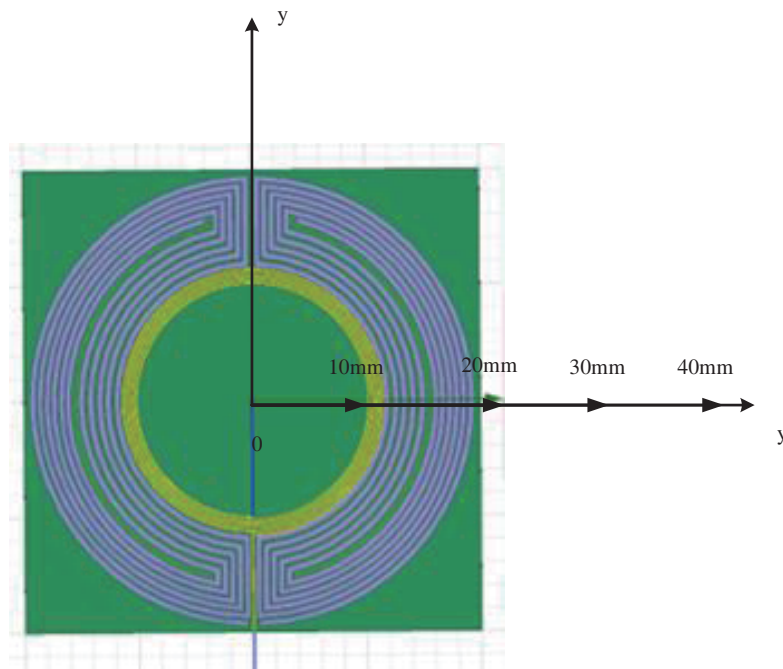

Figure 7. Magnetic field test points set up on a coil model using Maxwell equations.

4.2. Analysis Of Simulation Results

The corresponding LCC-P compensation circuit model is built using Simplorer, and the circuit is introduced into the magnetic field interface and connected to the coil model for field coupling. The coil magnetic field distributions are obtained at coil spacings of 4 mm, 7 mm, and 10 mm as shown in Figures 8–10.

Comparing the magnetic induction strengths of the structures through 3D finite element
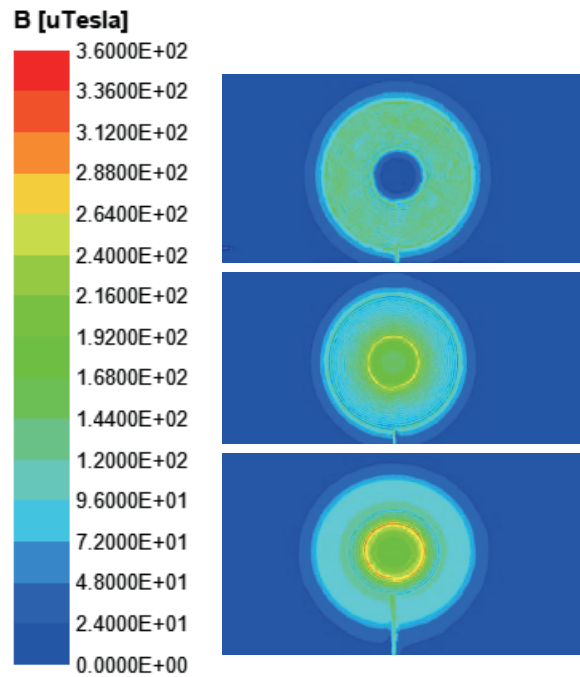
Figure 8. Top view of the receiving coil flux density distribution at 4 mm coil spacing.
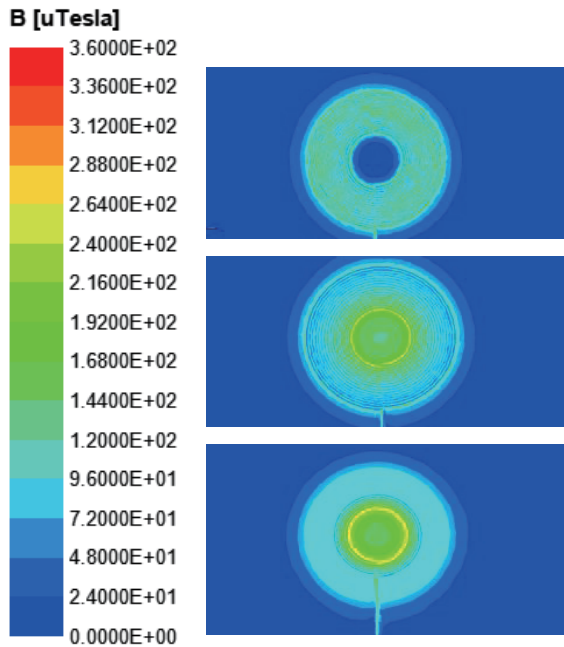

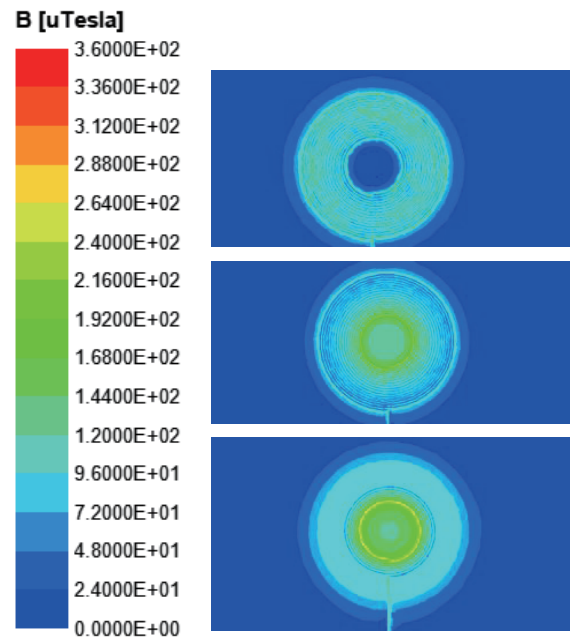**Figure 9.** Top view of the receiving coil flux density distribution at 7 mm coil spacing.

Figure 10. Top view of the receiving coil flux density distribution at 10 mm coil spacing.

simulations, the magnitude of the magnetic field outside the coil is greatly reduced when the proposed coil is applied. As can be seen from the numerical results in Table 1, the flux density distribution is significantly denser in the plane with a distance of 4 mm than that of the conventional receive-receive coil. The flux density in the central area is increased by 16%, while in the peripheral area it is reduced by 33%. This is due to the special configuration of the additional coils. The inner winding of the coil

Table 1. Transmission efficiency at different distances.

Distance/mm	Coil markings	Magnetic field acquisition data (μT)				
		0 mm	10 mm	20 mm	30 mm	40 mm
4 mm	1	11.9	12.6	10.8	6.7	1.6
	2	18.5	22.8	15.6	8.5	2.7
	3	20.4	24.3	14.2	6.5	1.8
7 mm	1	8.5	10.7	9.4	5.3	1.2
	2	15.7	20.1	12.4	7.2	2.0
	3	17.6	21.4	11.7	4.9	1.1
10 mm	1	6.2	8.8	8.1	4.5	0.9
	2	13.3	19.1	10.9	6.5	1.3
	3	14.2	18.5	9.6	3.7	0.7

is in the same direction as the receiving coil, and the outer winding is in the opposite direction to the receiving coil.

As a result, the flux density in the inner area is enhanced, and the flux density in the outer area is weakened by the in-phase current, thus allowing better use of the flux density. The magnetic field in other unnecessary areas within the electronic device is effectively limited. For planes at distances of 7 mm and 10 mm, the flux density of the coils is reduced by varying degrees beyond 20 mm in the horizontal position. The maximum value of the magnetic flux density in the plane of interest is reduced by more than 20%, verifying the effectiveness of the proposed coil in limiting the magnetic flux.
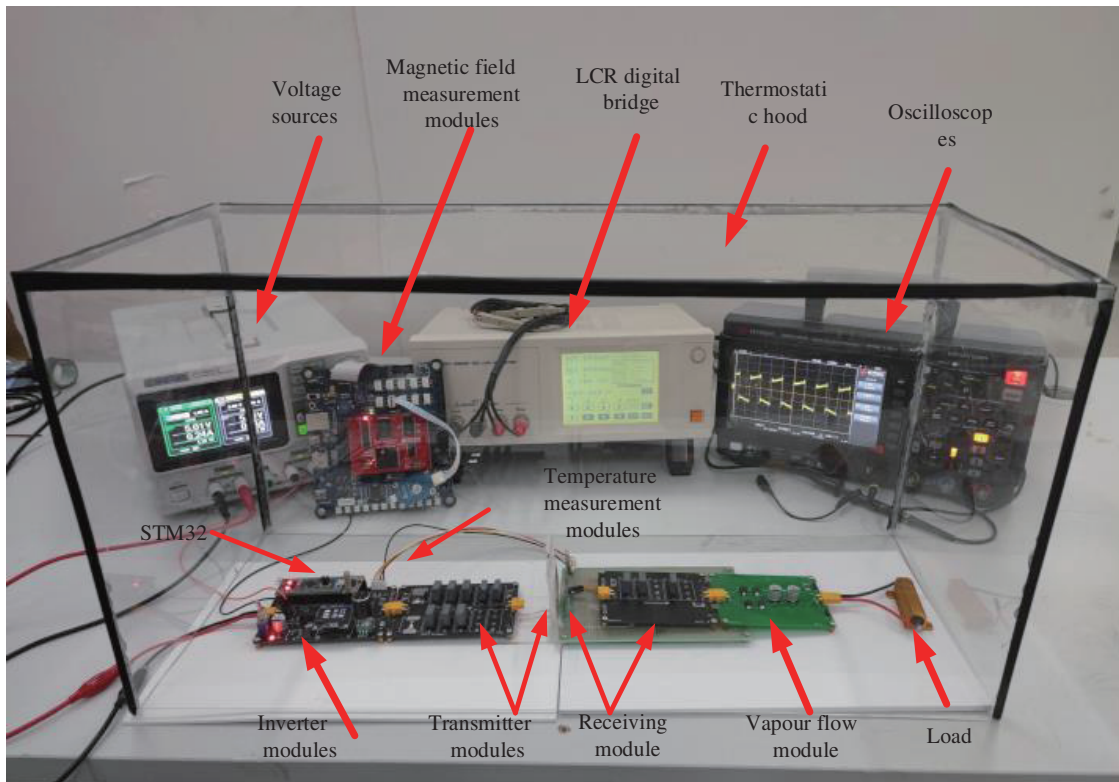

Figure 11. Experimental platform based on LCC-P compensation circuit at 100 kHz.

5. EXPERIMENTAL VERIFICATION

5.1. Experimental System Construction

Through the above analysis of the circuit and the analysis of the whole system model based on electromagnetic field theory, the resonant wireless energy supply experimental platform with double-layer receiver coupler designed in this paper was built as shown in Figure 11. The whole system consists of a DC power source, inverter module, transmitter module, receiver module, rectifier module, magnetic field measurement module, temperature measurement module, load resistor, and several other parts. The coil applied to the experiment is shown in Figure 12. Taking mobile phone wireless power supply as an example, the power source provides 5 V DC voltage to the inverter module. After inversion, the inverter module outputs AC 100 kHZ voltage. Set the impedance of the LCC-P compensation circuit to match. The inducted voltage of the receiver coil is rectified by the transmitter module. A 10 Ω power resistor is used as the equivalent substitution of the load. In order to reduce the influence of external factors on the charging and temperature measurement experiments, a nearly airtight space with a volume of 60 cm × 20 cm × 25 cm was constructed using a 2 mm thick acrylic board. The proposed double-layer receiver coupler was tested on the basis of this experimental validation platform, and the performance of the system was verified based on the experimental results and the analysis of the experimental data.
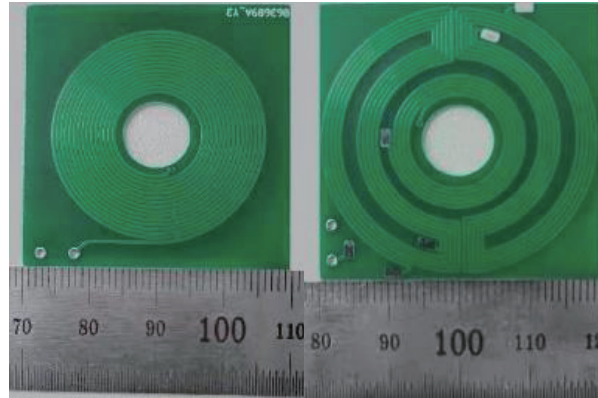

Figure 12. PCB coil model with additional coils.

5.2. Efficiency Tests

When the system works, the transmitter coil and receiver coil are perfectly aligned, and the distance between the coils is relatively fixed. Taking a mobile phone as an example, the distance between the transmitter coil and receiver coil is set to be about 4 mm, and the coil parameters and circuit parameters are shown in Table 2 and Table 3, respectively.

Table 2. Coil parameters.

Parameters	Numerical values			
	Inductors/μH	Number of turns	Inner diameter/mm	Outer diameter/mm
Transmitting coil	12.4	20	12	40
Receiving coil	9.37	15-5 Series	12	31.2
Additional Coils	3.4	5	28	40

For the resonant wireless energy supply system designed in this paper, the variation of transmission efficiencies under different transmission distances of 4 mm, 7 mm, 10 mm, 13 mm, and 16 mm are studied to test the overall performance of the system. The input/output voltage/current waveforms collected in the experiment are shown in Figure 13.

Table 3. System circuit parameters.

Parameters	L11/µH	C1/nF	C11/nF	CS/nF	K
Simulation values	6.8	372.5	452	270	0.45
Measured values	6.75	374	454.1	272.2	
Frequency			100 kHz		

Table 4. Transmission efficiency at different distances.

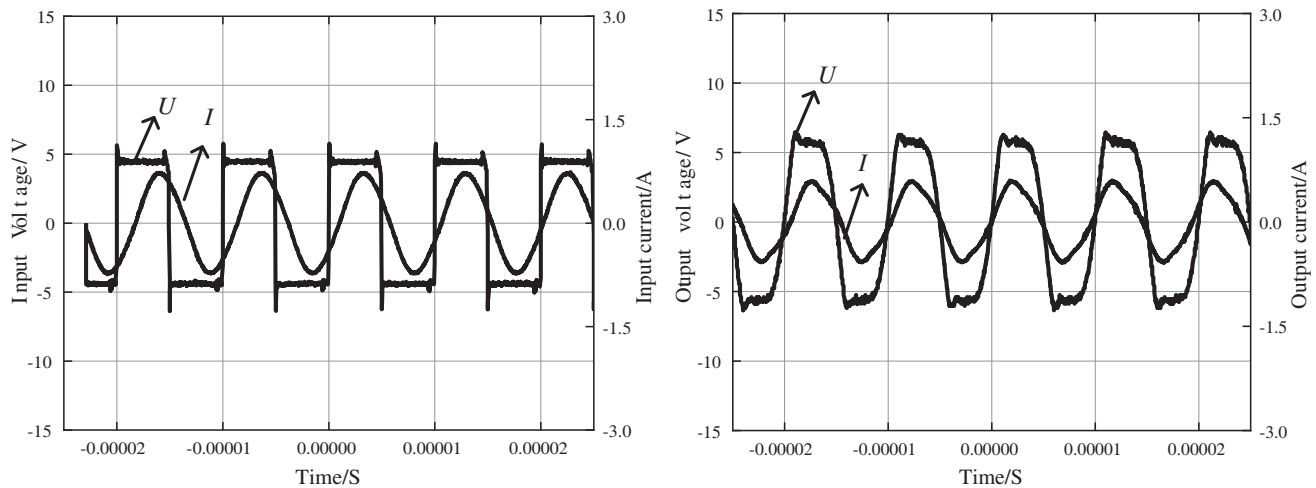| Distance/mm	Input			Output			Transmission efficiency/%
	Voltage/V	Current/A	Power W	Voltage/V	Current/A	Power/W	
4	4.47	0.55	2.46	4.04	0.43	1.74	71%
7	4.37	0.56	2.45	3.82	0.41	1.56	64%
10	4.46	0.52	2.32	3.75	0.32	1.20	52%
13	4.42	0.45	1.99	2.98	0.30	0.89	45%
16	4.34	0.36	1.56	2.84	0.22	0.62	40%

Figure 13. Experimentally measured input (output) voltage (current) waveforms.

From Table 4 it can be concluded that at a distance of 4–16 mm, the transmission efficiencies of the experimental system can reach 40%–71% under the configuration of the parameters designed in this paper, which meet the general charging requirements.

The mutual inductance between the coils in the WPT system was measured in the experiment at different distances as shown in Table 5, where T represents the transmitting coil; R represents the transmitting coil; a and b represent the additional coils.

As can be seen from the current waveforms in Figures 14 and 15, under the conditions set, although there are some errors caused by the system, the phases of the secondary side current and the additional coil current are the same. Both currents lag the transmitting coil current by 90° in phase.

5.3. Comparative Analysis

The following comparative experiments were done with different receiver coil configurations, the first with a single 15-turn PCB coil, the second with a 15-turn, 5-turn series PCB coil, and the third with a

Table 5. Coil mutual inductance at different distances.

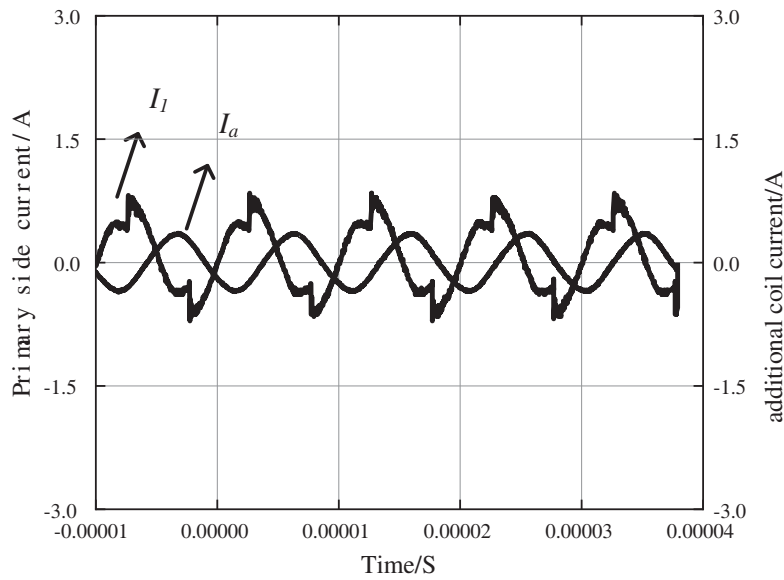| Distance/mm	Numerical values/μH		
	T-R	T-a	T-b
4	3.825	0.398	0.396
7	2.375	0.383	0.385
10	1.90	0.343	0.342
13	1.40	0.330	0.329
16	1.0	0.322	0.320

Figure 14. Phase of current between primary side current and additional coil.
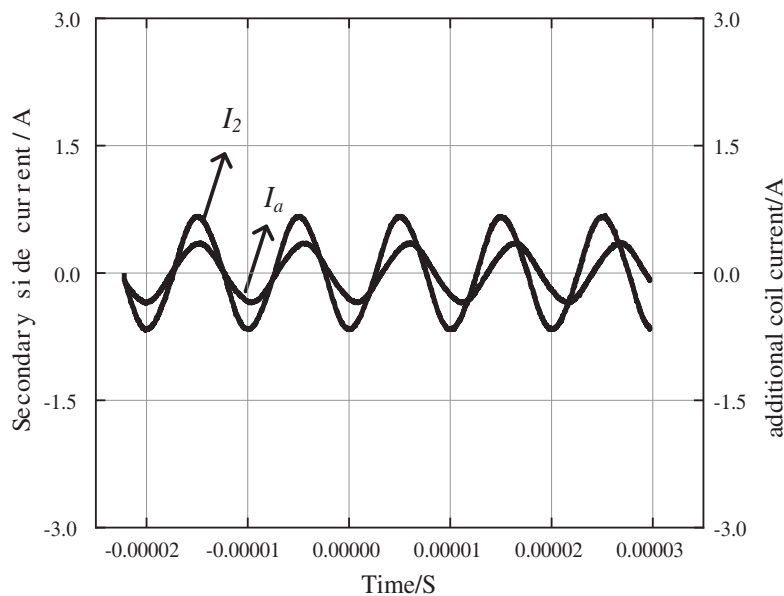

Figure 15. Phase of current between secondary side current and additional coil.
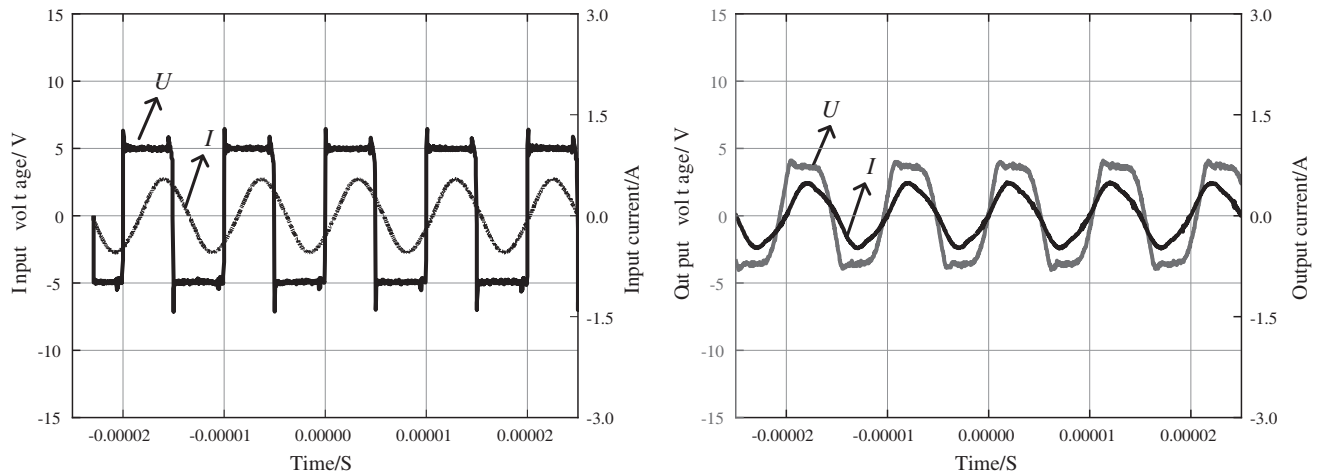
Figure 16. Input (output) voltage (current) waveforms obtained from the first set of experiments.
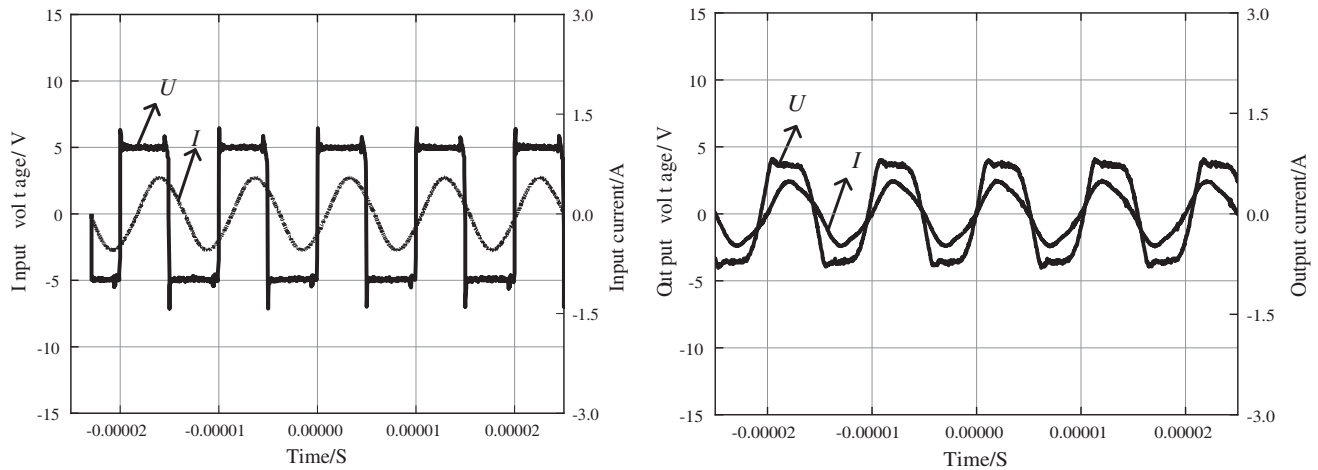

Figure 17. Input (output) voltage (current) waveforms obtained from the second set of experiments.

15-5 turn series PCB coil with additional coils to verify the correctness of the aforementioned theory.

The peak input/output voltages/currents of the three sets of experiments are shown in Figures 13, 16, and 17, and the results are shown in Table 6. By analyzing the experimental data, it can be found that at a distance of 4 mm, when the transmitting coils are aligned in the center of the coils, the double layer coils can improve the transmission efficiency better than the single layer coils. And the double layer receiving coils with additional coils have little effect on the overall system efficiency, which only changes by 2%.

Therefore, the proposed double-layer receiving coil with additional coils in this paper can effectively reduce the magnetic leakage on the receiving side without affecting the transmission efficiency. The transmission efficiency is 71%, which is a large improvement compared to the flexible PCB coil proposed in the paper [23], and no additional space was occupied.

5.3.1. Magnetic Field Analysis

Experimental analysis of the magnetic field was carried out for the three groups of experimental solutions, and experimental verification was carried out under the same conditions. The experimental data was collected at the same point as the simulation, and the magnetic field strengths at different

Table 6. Experimental results of 4 mm distance.

	Input			Output			Transmission efficiency/%
	Voltage/V	Current/A	Power/W	Voltage/V	Current/A	Power/W	
Group 1	4.41	0.51	2.24	2.95	0.48	1.42	63%
Group 2	4.45	0.53	2.36	3.99	0.43	1.72	73%
Group 3	4.47	0.55	2.46	4.04	0.43	1.74	71%
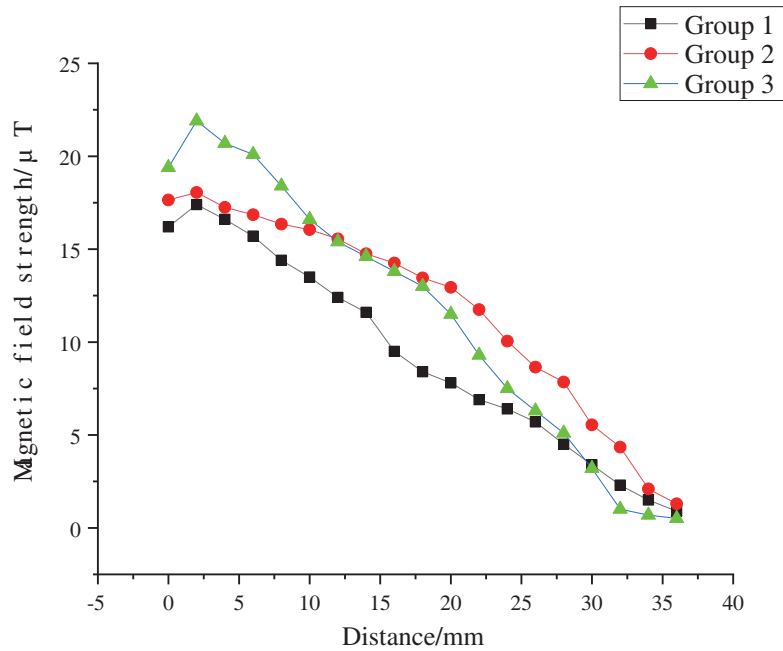
Figure 18. Experimentally measured magnetic field strength at different locations of the receiver coil attachment.

locations for the three groups of experiments are shown in Figure 18. Analyzing the experimental data collected from the three groups, it can be found that the magnetic field of the third group of coils is higher at 0–10 mm from the center of the coil than the other two groups of coils, and after 10 mm, the magnetic flux is smaller in the third group at the same position than the second group. The total external magnetic field is significantly reduced by the maximum of 53%. This demonstrates that the proposed double layer receiver coil with additional coils can significantly reduce the external magnetic flux level and the damage caused by the magnetic field to other electronic devices.

Figure 19 shows a comparison of the simulated and measured magnetic fields obtained with the three sets of coils located at the observation point shown in Figure 8. The measured data correlates well with the simulation results, and the simulation results have the same trend as the measured ones. Simulated and experimental results verify the advantages that the external magnetic field can be attenuated by the proposed coil.

5.3.2. Temperature Measurement Experiments

Construct an enclosed space of 2 mm acrylic panels and measure 60 cm × 20 cm × 25 cm, over the entire wireless charging system model to reduce interference from external factors. The temperature sensor is fixed to the receiver coil, and the temperature rise of the system is measured at the bottom of the
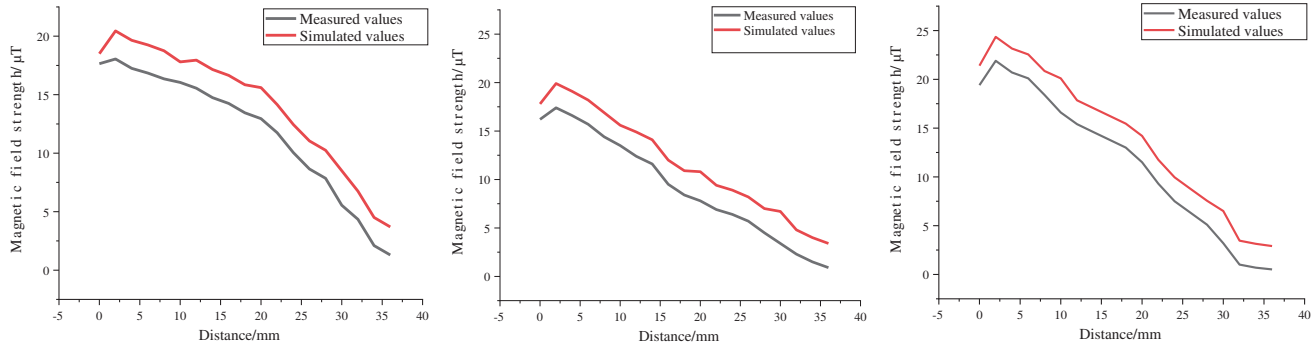
Figure 19. Comparison of simulated and measured values of magnetic field distribution for three sets of coils.

receiver coil, where the temperature rises the fastest.

The coupling coil is a key part of efficient energy transfer. The temperature rise of the coil caused by heat loss has a direct impact on the safe and efficient operation of the system over a long period of time, and the problems caused by overheating of the coil can directly threaten the safe and smooth operation of the system.

As shown in Figure 20, the initial temperature of the first group was 19.8°C at the time of charging and gradually increased as the charging time increased, eventually reaching 24.0°C at 60 min. The temperature rise was 4.2°C. The initial temperature of the second group was 19.7°C and reached 24.3°C at 60 min. The temperature rise was 4.6°C. The third group started at 19.3°C and reached 24.8°C at 60 min. The temperature rise was 5.5°C.
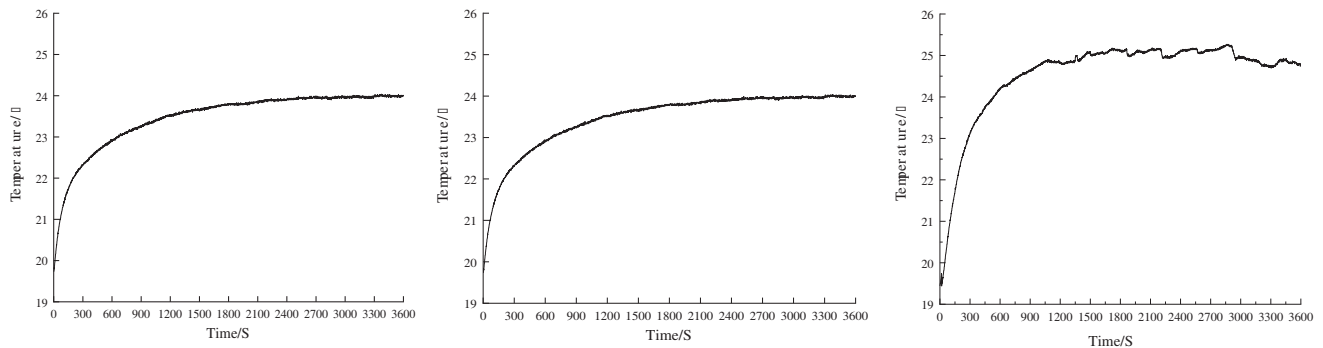

Figure 20. Temperature change of three sets of coils during 60 minutes of charging.

Therefore, it can be seen from the temperature rise results that the additional coils present in the third group of experiments did not unduly affect the overall temperature rise of the coils compared to the second group, and the differences in temperature rise among the three groups were not significant, as the first group had the lowest temperature rise due to the number of turns of the coils. This was because of the additional coils, but the temperature rise was only 1.3°C higher, meeting the requirements for system safety.

6. CONCLUSION

In this study, a wireless charging system is designed for the application in portable electronic devices. To reduce the influence of the magnetic field on the receiving side on the electronic components, a double-layer receiving coil with additional coils is proposed. The main work and conclusions of this paper are as follows: A circuit model for a system with a double-layer receiver coil based on an LCC-P compensation circuit at 100 kHz is used. The analysis of the magnetic field distribution of different coils

at different transmission distances shows that the magnetic field of the proposed coil structure is reduced to different degrees at different locations from the outside of the receiving coil at different transmission distances, verifying the safety of the system. At a frequency of 100 kHz, the use of a double-layer receiver coil structure with additional coils significantly reduces the magnetic field strength near the secondary side of the WPT system while maintaining transmission efficiency, thus reducing the influence of the edge field on the electronic components. At the center of the coil, the magnetic flux density rises by 16% and the external magnetic field strength is reduced by 20%. The temperature rises 5.34° during 60 min of charging, only 0.78° higher than the structure without additional coils.

ACKNOWLEDGMENT

REFERENCES

1. Tran, D. H., V. B. Vu, and W. Choi, "Design of a high-efficiency wireless power transfer system with intermediate coils for the on-board chargers of electric vehicles," *IEEE Transactions on Power Electronics*, Vol. 33, No. 1, 175–187, 2017.

2. Qu, X., H. Han, S. C. Wong, C. K. Tse, and W. Chen, "Hybrid IPT topologies with constant current or constant voltage output for battery charging applications," *IEEE Transactions on Power Electronics*, Vol. 30, No. 11, 6329–6337, 2015.

3. Takasaki, M., Y. Miura, and T. Ise, "Wireless power transfer system for gate power supplies of modular multilevel converters," *Power Electronics & Motion Control Conference IEEE*, 3183–3190, 2016.

4. Jang, Y. and M. M. Jovanovic, "A contactless electrical energy transmission system forportable-telephone battery chargers," *IEEE Transactions on Industrial Electronics*, Vol. 50, No. 3, 520–527, 2003.

5. Kim, S., J. S. Ho, and A. Poon, "Wireless power transfer to miniature implants: Transmitter optimization," *IEEE Transactions on Antennas & Propagation*, Vol. 60, No. 10, 4838–4845, 2012.

6. Campi, T., S. Cruciani, Palandrani, V. De Santis, A. Hirata, and M. Feliziani, "Wireless power transfer charging system for AIMDs and pacemakers," *IEEE Transactions on Microwave Theory & Techniques*, Vol. 24, No. 2, 633–642, 2016.

7. Kim, D., J. Park, B. Park, and Y. Shin, " Propulsion and rotation of microrobot based on a force on a magnetic material in a time-varying magnetic field using a wireless power transfer system," *IEEE Transactions on Magnetics*, Vol. 56, No. 1, 1–5, 2019.

8. Mutashar Abbas, S., M. A. Hannan, S. A. Samad, et al., "Design of spiral clrcular coils in wet and drytissue for bio-lmplanted micro-system applications," *Progress In Electromagnetics Research M*, Vol. 32, 181–200, 2013.

9. Xue, M. and Q. X. Yang, "Application status and key issues of wireless power transmission technology," *Transactions of China Electrotechnical Society*, Vol. 36, No. 8, 1548–1568, 2021.

10. Han, L. and L. Li, "Integrated wireless communications and wireless power transfer: An overview," *Physical Communication*, Vol. 25, pt. 2, 555–563, 2017.

11. Zhang, X., S. L. Ho, and W. Fu, "Optimal design and analysis of wireless power transfer system coupled with power source," *2015 IEEE International Magnetics Conference (INTERMAG)*, 2015.

12. Park, J., C. Park, Y. Shin, D. Kim, and B. Park, "Planar multiresonance reactive shield for reducing electromagnetic interference in portable wireless power charging application," *Applied Physics Letters*, Vol. 114, No. 20, 203902, 2019.

13. Barretto, E., N. Chavannes, and M. Douglas, "Challenges in safety and compliance assessment in wireless power transfer applications using numerical analysis: Guidelines and solutions," *European Conference on Antennas & Propagation IEEE*, 1–5, 2016.

14. Zhang, B. and X. J. Shu, "Urgent problems and countermeasures for wireless energy transmission technology," *Automation of Electric Power Systems*, Vol. 43, No. 18, 1–20, 2019.

15. Riehl, P. S., A. Satyamoorthy, H. Akram, Y. C. Yen, J. C. Yang, and B. Juan, "Wireless power systems for mobile devices supporting inductive and resonant operating modes," *IEEE Transactions on Microwave Theory & Techniques*, Vol. 63, No. 3, 780–790, 2015.

16. Hua, B, I. Yasar, and S. Lei, "Mobile phone mid-range wireless charger development via coupled magnetic resonance," *IEEE Transportation Electrification Conference & Expo*, 1–8, 2016.

17. Jia, J. L. and X. Q. Yan, "Research tends of magnetic coupling resonant wireless power transfer characteristics," *Transactions of China Electrotechnical Society*, Vol. 3, No. 20, 4217–4231, Oct. 2020.

18. Fan, X., X. Mo, and X. Zhang, "Overview of research status and application of wireless power transmission technology," *Transactions of China Electrotechnical Society*, Vol. 34, No. 7, 1353–1380, 2019.

19. Du, Y. P., T. C. Cheng, and A. S. Farag, "Principles of power-frequency magnetic field shielding with flat sheets in long conductors," *IEEE Transactions on Electromagnetic Compatibility*, Vo. 38, No. 3, 450–459, 1996.

20. Chen, K. N. and Z. M. Zhao, "Analysis of the double-layer printed spiral coil for wireless power transfer," *Emerging and Selected Topics in Power Electronics*, Vol. 1, No. 2, 114–121, 2013.

21. Li, Z., X. He, and Z. Shu, "The design of coils on printed circuit board for inductive power transfer system," *IET Power Electronics*, Vol. 11, No. 15, 2515–2522, 2018.

22. Li, J. and D. Costinett, "Analysis and design of a series self-resonant coil for wireless power transfer," *2018 IEEE Applied Power Electronics Conference and Exposition (APEC)*, 1052–1059, 2018.

23. Jeong, S., D.-H. Kim, J. Song, H. Kim, S. Lee, C. Song, J. Lee, J. Song, and J. Kim, "Smartwatch strap wireless power transfer system with flexible PCB coil and shielding material," *IEEE Transactions on Industrial Electronics*, Vol. 66, No. 5, 4054–4064, 2018.

24. Yi, Z, M. Li, B. Muneer, G. He, and X.-X. Yang, "Self-resonant antisymmetric planar coil for compact inductive power transfer system avoiding compensation circuits," *IEEE Transactions on Power Electronics*, Vol. 36, No. 5, 5121–5134, 2020.

25. Narayanan, R., "Advances in wireless power coils: The key element in a wireless power charging system," *IEEE Power Electronics Magazine*, Vol. 2, No. 4, 40–46, 2015.

26. Tang, X., H. Su, and H. Zhang, "Researches of a new coreless printed circuit board planar inductor," *Chinese Journal of Electron Devices*, Vol. 25, No. 4, 319–323, 2002.